JOURNAL OF APPLIED PHYSICS **116**, 084105 (2014)

Electric field and humidity effects on adsorbed water behavior on $BaTiO_3$ ferroelectric domains studied by scanning probe microscopy

D. Y. He,[1] L. J. Qiao,[1,a)] Mehdi Khodayari,[2] and Alex A. Volinsky[2,b)]
[1]*Corrosion and Protection Center, Key Laboratory for Environmental Fracture (MOE), University of Science and Technology Beijing, Beijing 100083, People's Republic of China*
[2]*Department of Mechanical Engineering, University of South Florida, Tampa, Florida 33620, USA*

(Received 25 June 2014; accepted 14 August 2014; published online 28 August 2014)

Distribution of the adsorbed water on $BaTiO_3$ ferroelectric single crystal (001) surface was investigated by means of scanning probe microscopy. Under high relative humidity, above 95%, the presence of water droplets was observed on domain surfaces. The droplets were up to 20 nm high and their morphology changed when electrical field was applied between the single crystal substrates and droplets via scanning probe microscopy. With an electric field applied parallel to the (001) top surface, the droplets on ***c*** domains spread out, followed by complete recovery upon switching the electric field off. However, few droplets on ***a*** domains tend to shrink with the electrical field application. It is shown that the screening surface charges and induced charges on droplets surface play a dominant role in droplets behavior. © *2014 AIP Publishing LLC*.
[http://dx.doi.org/10.1063/1.4894006]

INTRODUCTION

Humidity affects ferroelectrics performance. For oxide ceramics, like Al_2O_3, ZrO_2, and $YBa_2Cu_3O_7$, delayed fracture under sustained stress in humid air and water can occur, called stress corrosion cracking (SCC).[1–3] For ferroelectric ceramics, like $PbZr_{1-x}TixO_3$ (PZT) and $BaTiO_3$, SCC could also occur in humid air, due to adsorption and decreased surface energy.[4–6] On the other hand, delayed cracking of PZT ceramics in humid air could occur under sustained electric field, which is essentially one kind of SCC.[7,8] In contrast, the delayed crack propagation does not occur in dry air. During the ferroelectric operation in humid conditions, after long-term stress or electric field exposure, cracks may nucleate and propagate. Cracks in ferroelectrics can result in devices degradation. Humidity also affects ferroelectric polarization, inducing domain switching in dry conditions. Under mechanical stress or electric field in $BaTiO_3$ single crystal, humidity can promote domain switching from ***a*** to ***c***, but retard switching from ***c*** to ***a***.[9] The service and the failure of ferroelectrics are affected by the relative humidity. Understanding the interaction of water with the ferroelectric surface is important for identifying the SCC mechanisms.

The adsorption of water on ferroelectric surfaces in ambient conditions is of great interest.[10–14] In humid atmosphere, the small water droplets, which adsorb on the material surface, cause delayed cracking and fracture of ferroelectric ceramics.[15,16] The study of the water adsorption phenomena at the nanoscale is important for the advance in the fundamental understanding of ferroelectrics properties. Thus, it is useful to study the water droplets behavior. Understanding water adsorption, distribution and evolution will benefit the related ferroelectrics applications.

Water adsorption behavior is affected by both internal factors[17,18] (domain surface properties) and external factors[13,19,20] (light, thermal, electric, and magnetic fields, etc.). In the last decade, water adsorption on ferroelectrics has been widely studied by theoretical, experimental and computer simulation approaches to understand the adsorption behavior on surfaces.[18,21] In a previous study,[17] the intrinsic surface energy of the domain surface was measured, showing that after the ambient environment suddenly changed to an ultrahigh humidity, the water droplets appeared only on the ***c*** domain surfaces, preferred adsorption location for the water droplets. The adsorption of polar H_2O molecules not only reduced the surface energy but also the electrostatic energy of the ***c*** domains.[9] An external field can be applied to the given system without modifying its properties, which can be employed to study ferroelectrics properties. Among these external factors, the applied electric field offers promising means to study ferroelectrics, since under a certain electric field, domain switching would happen.[22,23] Ferroelectric perovskite oxide domain patterns are related to spontaneous polarization. Charges are screened on polarized ferroelectric surfaces and the surface charge dynamics affects the domain electric performance. Screening of the surface charges is a crucial phenomenon in ferroelectrics. Kalinin *et al*. observed the temperature-induced potential inversion on the $BaTiO_3$ (001) single crystal surface.[24] Bonnell *et al*. reported surface charge effects on the characterization of the domain polarization surface potential and the domain destabilization measured by piezoresponse force microscopy (PFM).[25] In addition, theoretical, experimental and computer simulation approaches gave evidence that the screening behavior of the +/- ***c*** domains is different. Li *et al*. conducted the density functional theory (DFT) calculations by studying the CO_2 adsorption on both c^+ and c^- TiO_2-terminated $BaTiO_3$ (001)

a)Author to whom correspondence should be addressed. Electronic mail: lqiao@ustb.edu.cn, Telephone: +86 10 6233 4499; Fax: +86 10 6233 2345
b)volinsky@usf.edu, Telephone: 813-974-5658; Fax: 813-974-3539

surfaces containing 1/3 of the oxygen vacancies monolayer. It turns out that the CO_2 chemisorption mode is polarization dependent.[20] Thus, the surface charge and dipole response to an applied electric field is important for ferroelectrics. Water adsorption behavior change with the externally applied electric field should be taken into account.

Due to the adequate lateral and vertical resolution, scanning probe microscopy (SPM) has been utilized to characterize ferroelectric surfaces.[26–28] In this paper, the details of water adsorption on domain surfaces have been investigated by SPM. The work presented here shows that it is possible to directly observe the formation, location, and the inherent stability of water droplets on different domain surfaces. It was found that the water droplets preferred to assemble at the regions of the ***c*** domain surfaces, while only a few randomly distributed water droplets assembled on the ***a*** domain surfaces. This phenomenon is explained in terms of the interactions between the polarized ferroelectric ***c*** domain surfaces and polar water molecules. Another interesting result was the evolution of water droplets after an electric field was applied. Due to the interaction between the water molecules and the domain surfaces, the water droplets on the ***a*** and ***c*** domain surfaces display different behavior. Here, the effects of the externally applied electric field and the humidity on the domain surfaces allow for a wide range of interactions to be investigated.

EXPERIMENT

$BaTiO_3$ single crystal with $2 \times 5 \times 1\,mm^3$ dimensions was used in this study. The crystals were poled along the [100] direction to get the ***a*** domains on the (001) observed plane, and then the (001) surface was polished by diamond lapping pastes and a 50 nm colloidal silica suspension, until the roughness of the (001) surface was less than 1 nm. After that, to obtain a multi-domain structure, the $BaTiO_3$ crystal was partially poled along the [001] direction. This way, a $BaTiO_3$ polarized domain surface with 90° ***a–c*** domain corrugation structure on the surface was achieved. The sample was then kept at 100 °C in dry Ar gas for 30 min to remove the surface adsorbates and slowly cooled to room temperature. Peter *et al*. studied the surface adsorbates using X-ray photoelectron spectroscopy.[13] It turns out that a surface layer consisting of chemisorbates and physisorbates prevails on perovskites. The surface layer can be removed to a large extent by heating the sample under the ultra-high vacuum conditions. Thus, to further remove the surface adsorbates, the sample heat treatment was carried out.

The experiments were carried out at room temperature with an Agilent 5500 scanning probe microscope equipped with an environmental chamber (Agilent Technologies, Santa Clara CA, USA). The microscope head was enclosed in the chamber, which isolated samples in a controlled atmosphere. The humidity in the SPM environmental chamber was controlled by the external humid air generation system. By continually circulating dry Ar gas to generate water vapor, stable humidity was achieved. The relative humidity (RH) in the chamber was measured by a digital hygrometer.

In-situ continuous observation of the water droplet adsorption on the surface was achieved in the tapping AFM mode. The Nanosensor silicon tips (PPP-NCH) were used. The tip was operated at 280 kHz in the tapping mode, close to its peak resonant frequency of 300 kHz. Here, tip spring constant is 42 N/m and the typical normal force is 169 ± 42 nN. During scanning, the rate was 1 Hz, thus it took 6 min to complete a single image capture.

A large 60 μm x 60 μm scan of the domain areas containing both ***a*** and ***c*** domains was obtained first. Surface topography with corrugations is attributed to the adjacent ***a*** and ***c*** domains. The Kelvin probe microscopy mode was used to distinguish ***a*** from ***c*** domains, where the ***a*** domains with no surface charge on its surface showed no change and the polarized ***c*** domains with surface charge on its surface showed high surface potential. Then the tip was accurately positioned at different polarized domain zones to observe the water droplets adsorption behavior.

In this work, an external electric field (***E***) was applied paralleled to the (001) top surface. After attaining the equilibrium of the water droplets on the domain surface, the SPM measurements were conducted with different electric field applied. Fig. 1 shows schematics of the water droplets measurements. By coating silver paste electrodes on both sides of the sample, a voltage source was connected using copper wires. The *in-situ* response and the dynamics of the water droplets affected by the external electric field were measured.

RESULTS AND DISCUSSION

Tapping mode AFM was used to characterize water distribution on the (001) $BaTiO_3$ single crystal surface at 95% RH. Fig. 2 shows the AFM image of water droplets distribution on the $BaTiO_3$ (001) surface. Water droplets are likely to nucleate and grow on the ferroelectric surface. After exposure to the humid air, a few small water droplets nucleated on the (001) surface. Nucleated water droplets grew in size with new droplets emerging with time. Droplet height increased continuously with time, growing fast during the first 20 min, and then slowing down. After 160 min droplets no longer grew and achieved saturation. The equilibrium state was reached with the lateral droplet size ranging from 100 nm to 500 nm and the height ranging from 20 nm to 40 nm. Here, water droplets strongly adsorb on the $BaTiO_3$ (001) surface. It appears that only a few of the big water droplets formed on the ***a*** domains, while many more water

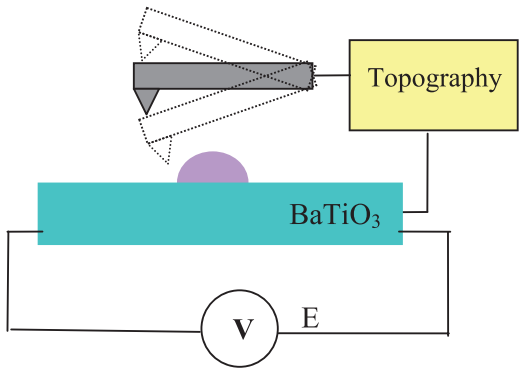

FIG. 1. Schematics of the domain surface water droplets measurements with electric field applied along the (001) $BaTiO_3$ surface.

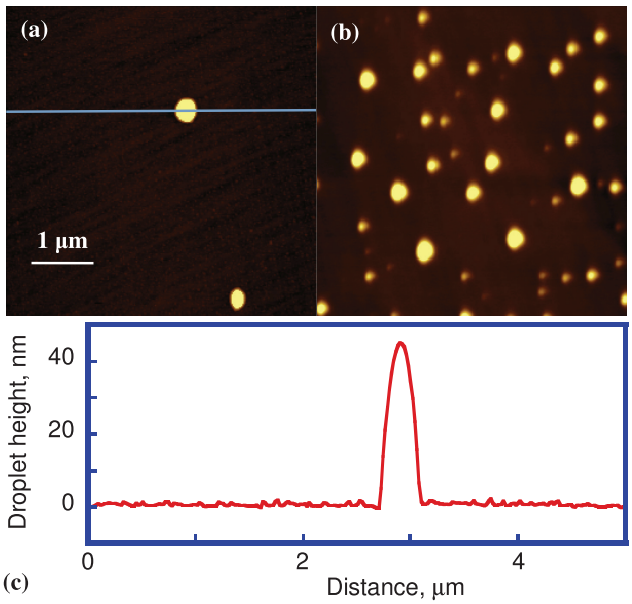

FIG. 2. Tapping mode AFM images (5×5 μm^2) of water droplets on the (001) $BaTiO_3$ single crystal surface taken at ambient conditions of 95% RH: (a) ***a*** domain surface and (b) ***c*** domain surface. Bright and round water droplets can be observed on the domain surface (50 nm Z scale); (c) The droplet topography section profile parallel to the applied electric field.

droplets assembled and spread on the ***c*** domains. Based on a typical topographical section profile in Fig. 2(c), the actual shape of water droplets was more like a disc paved on the domain surfaces, 40 nm high and up to 400 nm wide (Fig. 3(a)). Fig. 3(b) shows the Gaussian distribution of the droplets height assembled on the ***c*** domain. It appears that the size of over 80% of the droplets is between 20 nm and 22 nm. The spatial differentiation of the adsorbed water droplets between the ***a*** and ***c*** domains is due to their surface energy difference. Water adsorption on the ferroelectric surface is a spontaneous process associated with the surface energy change:

$$\boldsymbol{E} = (\boldsymbol{E_{Bulk}} + \boldsymbol{E_{H2O}} - \boldsymbol{E_{Bulk,H2O}}) > 0. \quad (1)$$

For the ***c*** domain surfaces, the polarization charge supplies additional electrostatic energy, thus the ***c*** domain has higher surface energy than the ***a*** domain, which is also demonstrated by the *ab initio* local density calculations.[29] Polar water molecules are more inclined to adsorb on the ***c*** domains to neutralize the surface charges. After long time exposure to the highly humid atmosphere, the ferroelectric surface is already saturated with H_2O with no significant surface energy change, resulting in water droplets widespread on the ***c*** domain surfaces, while scattered on the ***a*** domain surfaces.

The continuous changes of the water droplets on the ***a*** domain surface were observed while the applied bias was 10 V. Since the length of the sample was 5 mm, the external electric field intensity was calculated as 2 V/mm, as seen in Fig. 4. After the electric field was applied, the surface conditions changed remarkably, as the droplet volume kept contracting and both the lateral and the vertical size of the droplets was shrinking. The measured droplet height decreased continuously with time, changing fast at the first 25 min and then slowing down (Fig. 5). After 100 min, droplets were quite small and no longer changed. Due to the occasional drift during scanning, the same region was outlined in these images. The applied external electric field in humid air has a significant effect on the adsorbed water droplets on the ***a*** domain surface.

However, with the external electric field applied to the single crystal sample, the droplets on the ***c*** domain surface did not show exactly the same behavior as on the ***a*** domain. Fig. 6 shows the evolution of water droplets distribution on the (001) $BaTiO_3$ ***c*** domain surface as a function of the externally applied electric field intensity. In this case, continued scanning was conducted for 2 h for each value of the applied electric field, except for the 2 V/mm intensity. For the 2 V/mm, the droplets size evolution was different than at higher intensity, which will be discussed further. As the applied external electric field increased, the image contrast decreased and the water droplets boundaries became less pronounced with time. It appears that at the 6 V/mm applied electric field intensity, the two circled droplets almost joined. Three-dimensional plot of the water droplets in Fig. 7 shows that their morphology changed, and their height decreased significantly to only 1–2 nm, while the diameter increased. When the maximum 12 V/mm electric field intensity was applied, the contrast became too low to be distinguished. From the Gaussian distribution of the water droplets height in Fig. 8, it appears that the average height decreased with the applied electric field intensity. Without any electric field applied, 80% of the droplets had an average height of 20 nm. At the 2 V/mm electric field intensity, the droplet height reduced to 9 nm for 50% of the droplets. Eventually, at the maximum intensity of 12 V/mm, the height was between

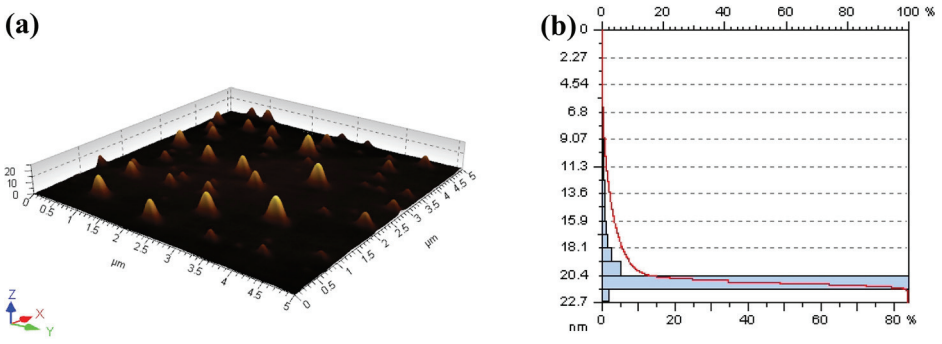

FIG. 3. (a) Three-dimensional plot of the water droplets on the (001) $BaTiO_3$ single crystal ***c*** domain surface; (b) Water droplets height Gaussian distribution.

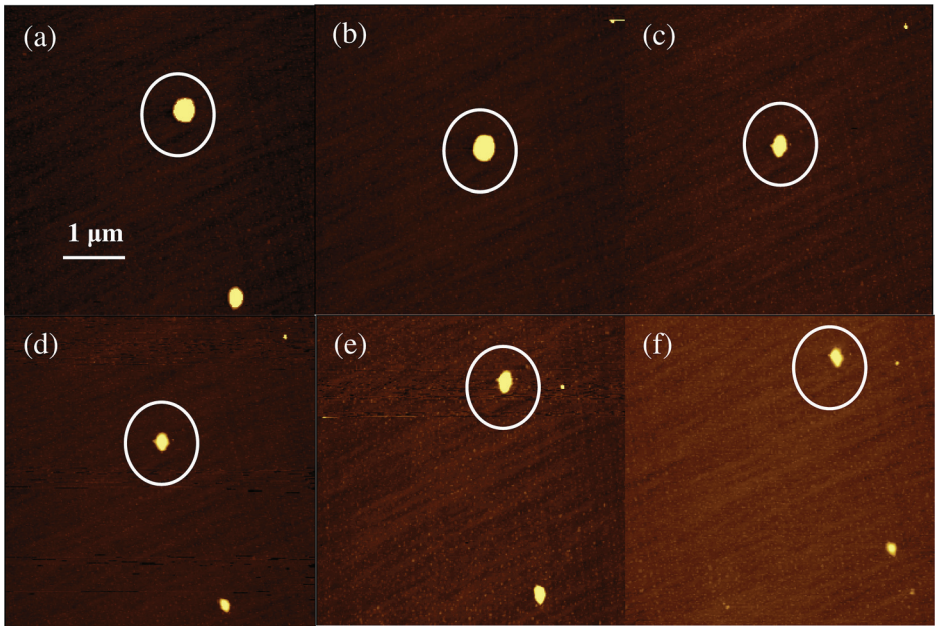

FIG. 4. Tapping mode AFM images of water droplets evolution on the (001) $BaTiO_3$ single crystal ***a*** domain surface (5×5 μm^2) with the 2 V/mm electric field intensity applied to the sample for: (a) 8 min, (b) 16 min, (c) 32 min, (d) 56 min, (e) 120 min, (f) 152 min.

0.5 nm and 2 nm, and the whole domain surface was completely covered by a water film. The fact that the diameter was always increasing suggests a similar behavior to electrowetting.[30–32] The strong electrostatic interaction between water and the ***c*** domain spreads the droplets on the surface for each electric field intensity condition. The time evolution of the droplets height is summarized in Fig. 9. Once the electric field intensity of 2 V/mm was applied to the sample, the water droplets height initially decreased very fast in a short period of time, from 20 nm to 6 nm, but then slowly increased to 17 nm in 320 min. The height continued to decrease with the applied electric field intensity, and always remained stable at each value. At the 8 V/mm intensity, the droplet height reduced to 2 nm.

To fully understand the external electric field effect on the water droplets, the symmetry of the droplets morphology was considered. Fig. 10 shows typical droplets' topography section profiles made either perpendicular or parallel to the externally applied electric field. It appears that the droplets remain symmetric in both directions. The shape changes mainly due to the surface physical and chemical properties, and the surface reaction with polar water molecules.

Although observed water droplets behavior on the $BaTiO_3$ single crystal domains happens at the nanoscale, to some extent, the observed nanoscale behavior is related to the surface wettability at the macroscopic scale, which has been successfully employed to study the surface wetting phenomena.[33,34] In order to figure out the nanoscale droplets behavior, the contact angle on the ferroelectric surface was also measured in this study. The contact angle measurement

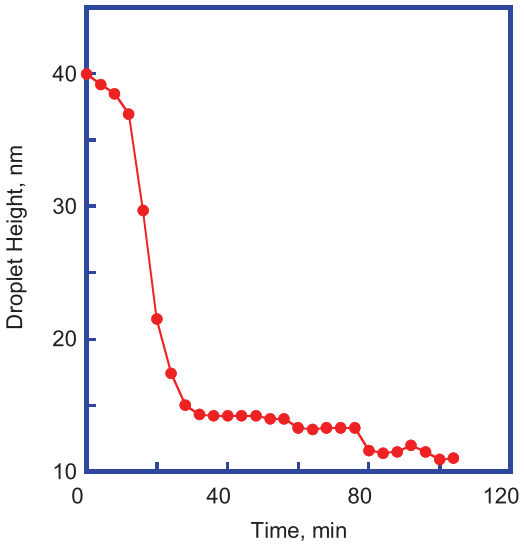

FIG. 5. Water droplet height time dependence after applying the 2 V/mm external electric field intensity.

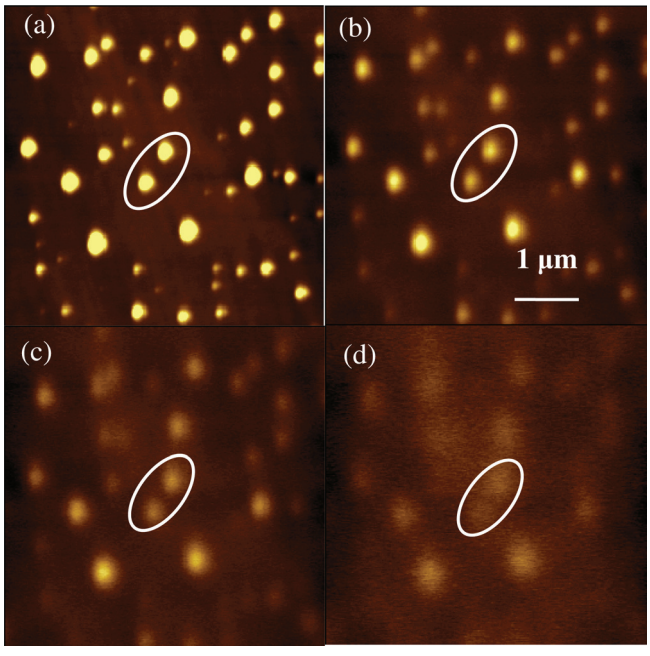

FIG. 6. Tapping mode AFM images of the water droplets distribution on the (001) $BaTiO_3$ ***c*** domain surface as a function of externally applied electric field intensity: (a) 0 V/mm; (b) 2 V/mm; (c) 4 V/mm; (d) 6 V/mm.

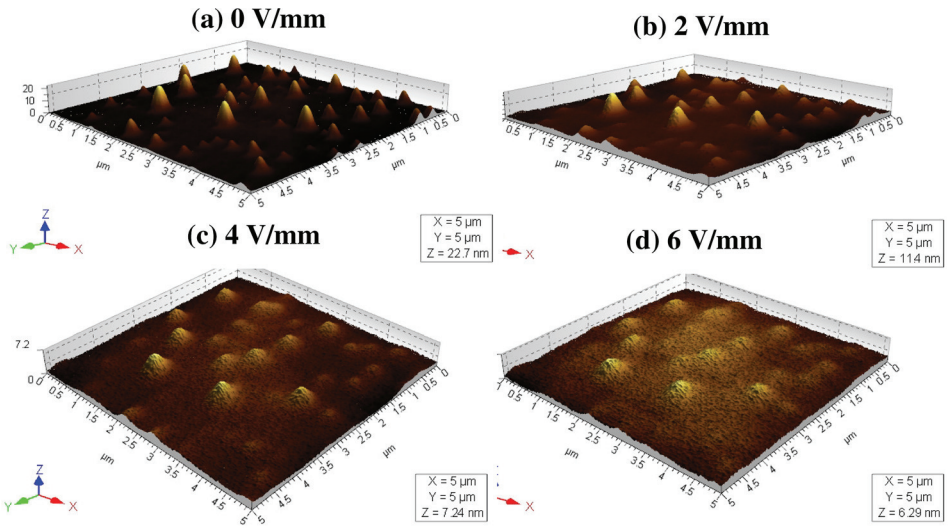

FIG. 7. Three-dimensional plots of the water droplets on the (001) $BaTiO_3$ single crystal ***c*** domain surface at different applied electric field intensity.

experiment was conducted in air at room temperature. The amount of water in the droplet was 0.4 μl. The contact angle shows an average value of 66.9°, indicating that the $BaTiO_3$ single crystal has a hydrophilic (001) top surface. Similarly, it appears in the captured AFM images that water tends to spread out on the ferroelectric surface. To analyze the evolution of water droplets on the ***c*** domain surface as a function of the externally applied electric field intensity, the height and the width of the droplets were also measured. Since the contact angle reflects the surface wettability, the angle at the solid liquid interface was acquired to analyze the electrowetting behavior in this case. In order to minimize the measurement error associated with the limited number of data points in the height profile (256 × 256 AFM images), only the values of droplets radius, a, and height, h, are presented (Fig. 11). The droplet is like a cap of a sphere with the radius r:

$$r = \frac{a^2 + h^2}{2h}. \tag{2}$$

Then, a and r can be used to find θ as

$$\cos(90^\circ - \theta) = a/r, \tag{3}$$

where θ is the apparent contact angle. Dimensions of three droplets were measured at positions A, B, and C as shown in Fig. 12.

Fig. 13 shows typical ***c*** domain droplet dimensions vs. the applied external electric field intensity. The angle continues to get smaller in Fig. 13(c), indicating a tendency for better water wettability. The droplets volume was calculated according to the half ellipsoid volume formula, which shows a declining tendency in Fig 13(d). The externally applied electric field induced a surface electronic reconstruction to

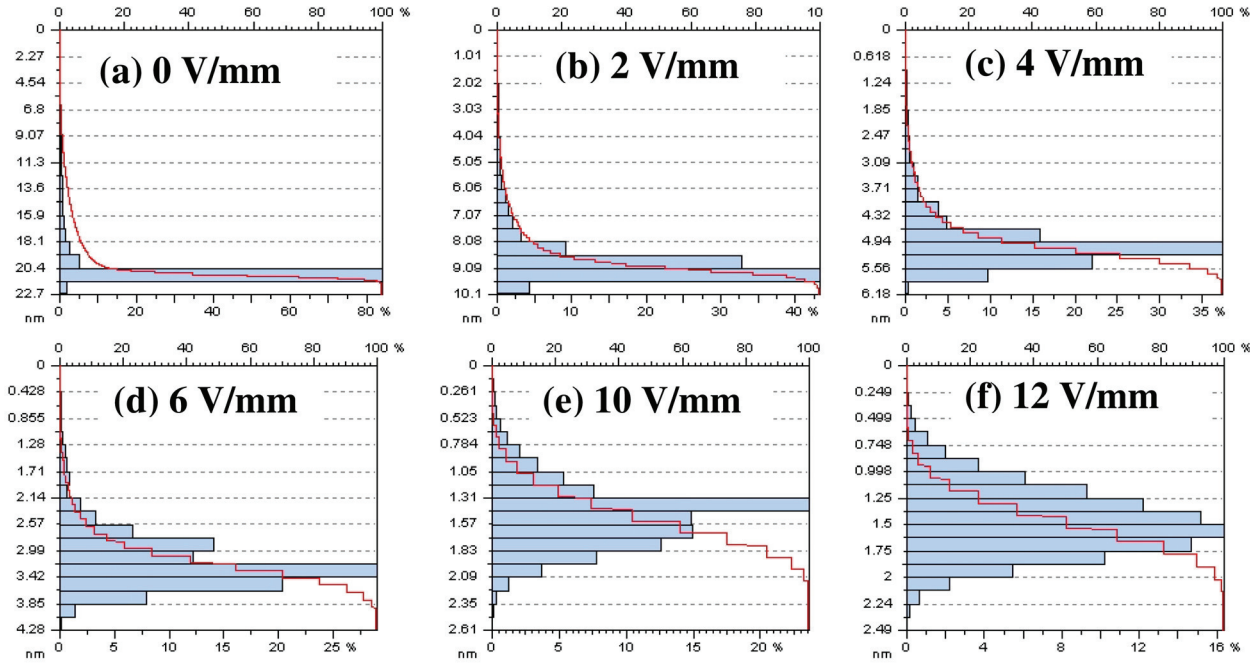

FIG. 8. The electric field intensity dependence of the water droplets height Gaussian distribution.

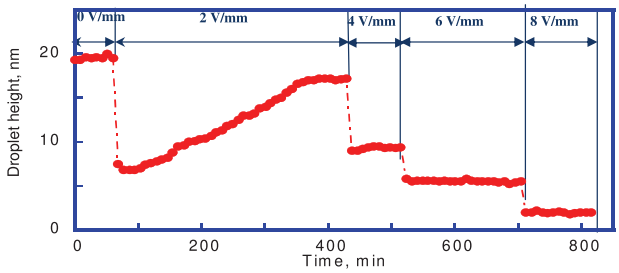

FIG. 9. Droplets height evolution with time obtained from the images in Fig. 6.

compensate the depolarizing field, increasing the polarized ***c*** domain surface energy. Thus, the electric performance of the surface adsorbed droplets changed.[18,35]

A complete recovery upon switching the electric field off has been observed, as seen in Fig. 14. Not only the location of the water droplets but also their shapes were restored to the original condition. The same thing occured as the intensity was reduced step by step to 2 V/mm. The captured images look exactly the same as the original droplets distribution with each electric field applied. This transition was found to be reversible, quite similar to the floating electrode electro-wetting.[36]

It is interesting to compare the difference of electric field and humidity effects on the ***a*** domain and the ***c*** domain surfaces. It appears that the observed droplets were strongly interacting with the surface due to the spontaneous adsorption of the water molecules on the ferroelectric surface. The water adsorption/desorption are quite sensitive to the externally applied electric field. This phenomenon can be linked to the intrinsic ferroelectric properties of the $BaTiO_3$ single crystal.

Polarization charge supplies the ***c*** domain surface with additional electrostatic energy, thus the ***c*** domain has higher surface energy than the ***a*** domain, which is also demonstrated by the *ab initio* local density calculations.[27] Polar H_2O molecules prefer to adsorb on the ***c*** domain to neutralize its surface charge, reducing the higher surface energy.[17] With longer humidity exposure, much of the adsorbed droplets assembled on the ***c*** domain surface, while only a few droplets assembled randomly on the ***a*** domain surface at certain sites.

Much effort has been dedicated to study the effects of the externally applied electric field on the surface adsorption.[36–39]

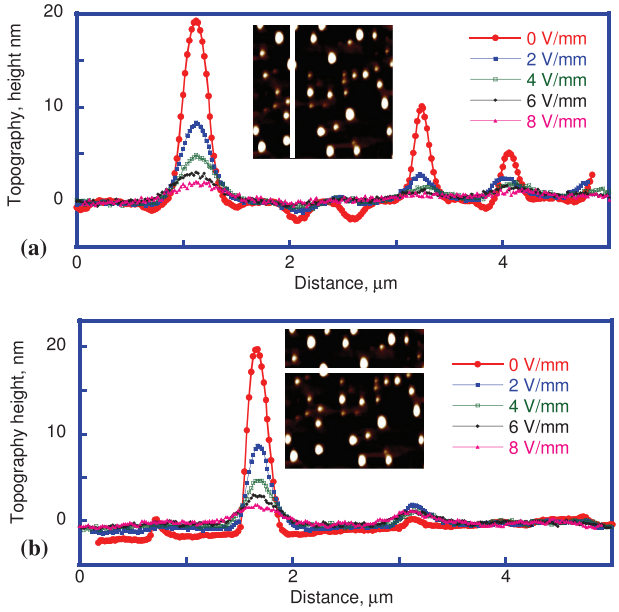

FIG. 10. The topography section height profile: (a) perpendicular and (b) parallel to the externally applied electric field.

After an electric field is applied to the sample, the apparent surface adsorption energy would change.[28] Density functional theory calculations show that positive electric field, corresponding to the positively charged surface, reduces the adsorption energy of the oxygen species on the Pt (111) planes, whereas negative field increases the adsorption energy.[37] With any increase in parallel electric field strength, the total energy and the adsorption energy values increase, inducing significant CO absorbtion on the AlN nanotubes.[38] The first principles study of the $PbTiO_3$ surface shows that an external electric field modifies surface reactions through the surface electronic reconstruction, where electrons or holes move to compensate the polarization-induced surface charge.[35] Here, the experimental results show that the electric field has a profound influence on the adsorption of water molecules on the ferroelectric surface.

The effect of the electric field on the surface droplets can be estimated from the physical properties of the $BaTiO_3$ single crystal. Ferroelectric ***c*** domains with polarization charge on the surface induce spatially selective photochemical effect[39] and photoexcitation[40] on its surface. The

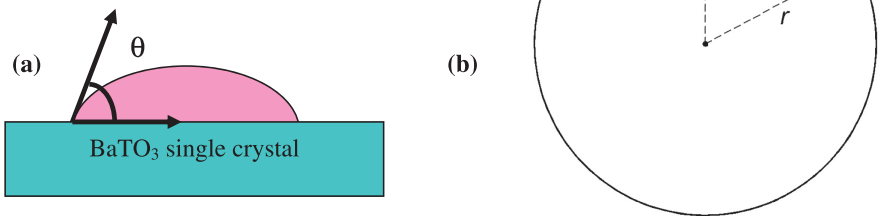

FIG. 11. Schematics of the angle related to the water droplets on the domain surfaces: (a) Standard contact angle; (b) The measured contact angle model.

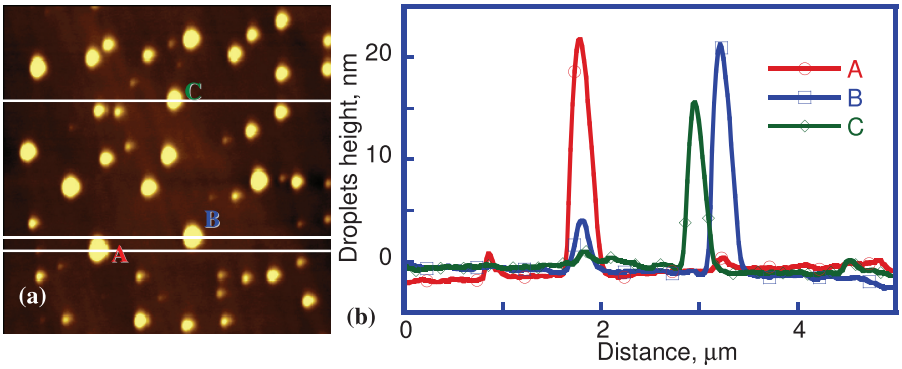

FIG. 12. (a) AFM image of water droplets on the (001) $BaTiO_3$ ***c*** domain surface. The selected positions are marked as A, B, and C; (b) The surface topography section profiles corresponding to each position parallel to the applied electric field.

spontaneous polarization of tetragonal $BaTiO_3$ is reported as 26 ± 3 $\mu C/cm^2$ at room temperature,[41,42] suggesting a compensating charge density of 0.37 e^-/surface unit cell when the dipole is perfectly screened. Under an applied electric field, the charged surfaces are subjected to the electrostatic forces along the direction of the applied electric field, resulting in surface charges changing the surface mechanical properties.[43] On the other hand, for the nanoscale water droplets, the effect of gravity can be negligible. The shape is mainly determined by the surface energy. After the nano-droplets are subjected to an external electric field, the induced charge is generated on the surface of the droplets, resulting in the additional electrostatic field. The effect of the surface charge and the induced charge result in increasing the total energy and the adsorption energy, which destabilize the water droplets. The achieved former balance has been broken. According to the principle of the surface free energy minimization, the water droplets tend to spread out on the surface. With the applied electric field and time, a new equilibrium is formed. Electric field externally applied to the ferroelectric sample would also cause some Joule heating.[44] Therefore, the droplets volume is partly decreasing, eventhough the adsorption continues in humid atmosphere. However, from 0 V/mm to 2 V/mm, the droplets' equilibrium state was broken. With the external force applied, the surface mechanical properties changed with initial decrease of the droplet height. The Joule heating accompanied by the applied in-plane electric field has a pronounced effect on this behavior. While the electric field is quite low, the effect is limited and stable. Beyond that, in the highly humid conditions, the water adsorption continues to reach a new equilibrium state. For the barium titanate oxide single crystal sample, the coercive

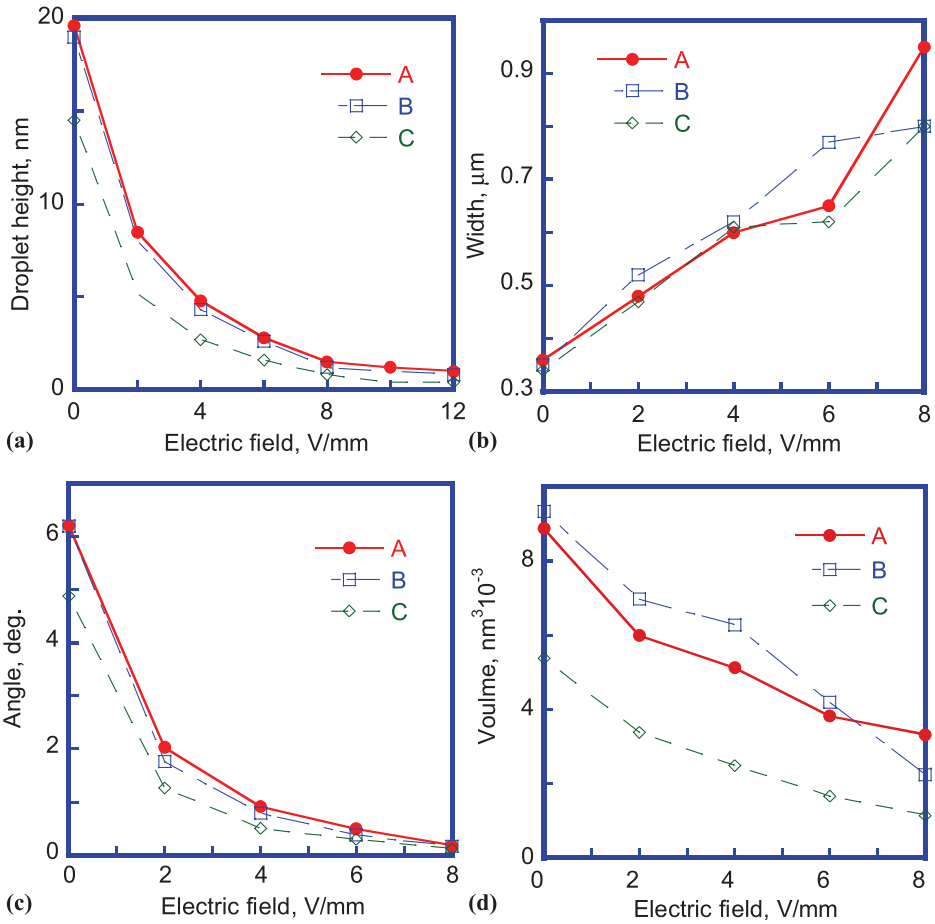

FIG. 13. (a) The droplets height and (b) The width (along the electric field direction); (c) The contact angle; (d) The droplets volume vs. the electric field intensity.

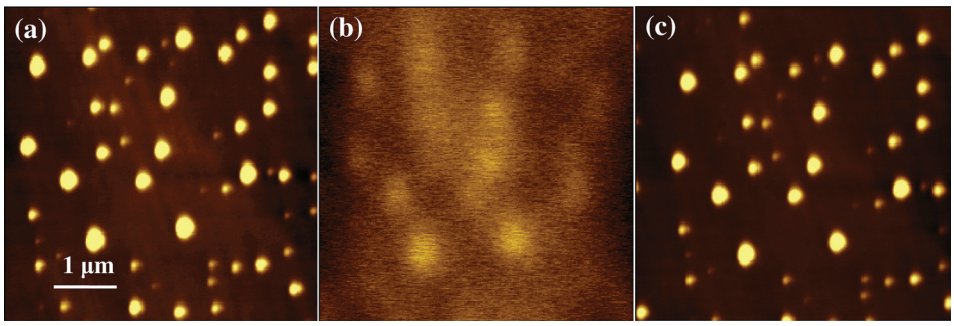

FIG. 14. (a) AFM local topography image of the droplets on the (001) $BaTiO_3$ surface without the electric field applied; (b) With a 12 V/mm electric field intensity applied; (c) Complete recovery upon switching the electric field off (20 nm Z scale).

value is 200 V/mm.[45] Although the maximum electric field intensity of 12 V/mm is still low compared with the 200 V/mm coercive field intensity, the effective electric field is still sufficient to modify the water droplets equilibrium state. When the electric field is switched off, the additional electrostatic energy change returns to the initial state. Again, in the 95% RH atmosphere, the surface droplets recover to the original volume and shape due to the water adsorption on the polar ***c*** domain surface. For the ***a*** domain, there is no screening charge on the surface. As a result, even though an electric field was applied to the sample, there was no mobile screening charge gathered. Thus, the adsorption energy decreased, and the droplets volume declined.

CONCLUSIONS

In summary, water interacts strongly with the $BaTiO_3$ (001) surface. Adsorption difference between the ***a*** and ***c*** domains is due to their different surface energy. Water droplets form preferentially on the ***c*** domain surfaces, resulting in more droplets on the ***c*** domain surfaces. The droplet evolution on the (001) $BaTiO_3$ single crystal surface with electric fields applied along the [010] direction was studied. A strong influence of the electric field on the droplet surface behavior was found. With the applied electric field, the measured droplet size on the ***a*** domains decreased continuously with time. However, on the ***c*** domains, the droplets tended to spread out on the surface as the applied electric field intensity increased and restored their shape when the electric field was turned off. This electric field-dependent water droplets behavior relies on the water adsorption and desorption on ferroelectric surfaces, indicating much stronger adsorption on the ***c*** domains. Applied electric field partially influenced the change of the surface droplets shape.

ACKNOWLEDGMENTS

Authors acknowledge support from the National Nature Science Foundation of China under Grant No. 512072021, the Program for the Changjiang Scholars, and the Innovative Research Team in the University (IRT1207). Alex Volinsky acknowledges support from the National Science Foundation under the IRES:1358088 grant.

[1]S. M. Spearing, F. W. Zok, and A. G. Evans, J. Am. Ceram. Soc. **77**, 562 (1994).
[2]J. E. Ritter and J. N. Humenik, J. Mater. Sci. **14**, 626 (1979).
[3]F. Oba, F. Ernst, Y. Yu, R. Liu, H. M. Kothari, and J. A. Switzer, J. Am. Ceram. Soc. **88**, 253 (2005).
[4]Y. Wang, W. Y. Chu, Y. J. Su, and L. J. Qiao, Mater. Sci. Eng. B **95**, 263 (2002).
[5]R. M. Wang, W. Y. Chu, K. W. Gao, Y. J. Su, and L. J. Qiao, Mater. Lett. **58**, 1811 (2004).
[6]Y. J. Su, Y. Wang, W. Y. Chu, K. W. Gao, and L. J. Qiao, Acta. Mater. **52**, 3753 (2004).
[7]Y. Wang, W. Y. Chu, K. W. Gao, Y. J. Su, and L. J. Qiao, Appl. Phys. Lett. **82**, 1583 (2003).
[8]H. Y. Huang, W. Y. Chu, Y. J. Su, L. J. Qiao, and K. W. Gao, Mater. Sci. Eng. B **122**, 1 (2005).
[9]B. Jiang, Y. Bai, W. Y. Chu, S. Q. Shi, L. J. Qiao, and Y. J. Su, Appl. Surf. Sci. **254**, 5594 (2008).
[10]G. A. Kimmel, N. G. Petrik, Z. Dohnálek, and B. D. Kay, Phys. Rev. Lett. **95**, 166102 (2005).
[11]K. B. Jinesh and J. W. M. Frenken, Phys. Rev. Lett. **96**, 166103 (2006).
[12]S. Gritschneder, Y. Iwasawa, and M. Reichling, Nanotechnology **18**, 044025 (2007).
[13]F. Peter, K. Szot, R. Waser, B. Reichenberg, S. Tiedke, and J. Szade, Appl. Phys. Lett. **85**, 2896 (2004).
[14]A. V. Ievlev, A. N. Morozovska, V. Ya. Shur, and S. V. Kalinin, Appl. Phys. Lett. **104**, 092908 (2014).
[15]B. Jiang, Y. Bai, J. L. Cao, Y. J. Su, S. Q. Shi, W. Y. Chu, and L. J. Qiao, J. Appl. Phys. **103**, 116102 (2008).
[16]X. Sun, Y. J. Su, K. W. Gao, L. Q. Guo, L. J. Qiao, and W. Y. Chu, J. Appl. Phys. **110**, 014103 (2011).
[17]D. Y. He, L. J. Qiao, A. A. Volinsky, Y. Bai, M. Wu, and W. Y. Chu, Appl. Phys. Lett. **98**, 062905 (2011).
[18]D. Dahan, M. Molotskii, G. Rosenman, and Y. Rosenwak, Appl. Phys. Lett. **89**, 152902 (2006).
[19]D. Y. He, L. J. Qiao, and A. A. Volinsky, J. Appl. Phys. **110**, 074104 (2011).
[20]D. B. Li, M. H. Zhao, J. Garra, A. M. Kolpak, A. M. Rappe, D. A. Bonnell, and J. M. Vohs, Nature Mater. **7**, 473 (2008).
[21]G. Geneste and B. Dkhil, Phys. Rev. B **79**, 235420 (2009).
[22]V. Nagarajan, A. Roytburd, and A. Stanishevsky, Nature Mater. **2**, 43 (2003).
[23]F. Xu, S. Trolier-McKinstry, and W. Ren, J. Appl. Phys. **89**, 1336 (2001).
[24]S. V. Kalinin, C. Y. Johnson, and D. A. Bonnell, J. Appl. Phys. **91**, 3816 (2002).
[25]R. Shao, M. P. Nikiforov, and D. A. Bonnell, Appl. Phys. Lett. **89**, 112904 (2006).
[26]O. S. Ovchinnikov, S. Jesse, and S. V. Kalinin, Nanotechnology **20**, 255701 (2009).
[27]S. V. Kalinin, A. N. Morozovska, L. Q. Chen, and B. J. Rodriguez, Rep. Prog. Phys. **73**, 056502 (2010).
[28]Y. B. Park, M. J. Dicken, Z. H. Xu, and X. D. Li, J. Appl. Phys. **102**, 083507 (2007).
[29]X. Y. Xue, C. L. Wang, and W. L. Zhong, Surf. Sci. **550**, 73 (2004).
[30]N. Crane, P. Mishra, and A. A. Volinsky, Rev. Sci. Instrum. **81**, 043902-7 (2010).
[31]N. Crane, A. A. Volinsky, P. Mishra, A. Rajgadkar, and M. Khodayari, Appl. Phys. Lett. **96**, 104103 (2010).
[32]N. B. Crane, A. A. Volinsky, V. Ramadoss, M. Nellis, P. Mishra, and X. Pang, Mater. Res. Soc. Symp. Proc. **1052**, DD8.1 (2008).
[33]Y. J. Yin and Ch. X. Wang, Colloids Surf. A **417**, 120 (2013).
[34]X. Sh. Zhang, B. Meng, F. Y. Zhu, W. Tang, and H. X. Zhang, Sens. Actuators, A **208**, 166 (2014).

[35]K. Garrity, A. Kakekhani, A. Kolpak, and S. I. Beigi, Phys. Rev. B **88**, 045401 (2013).
[36]M. Khodayari, B. Hahne, N. B. Crane, and A. A. Volinsky, Appl. Phys. Lett. **102**, 192907 (2013).
[37]M. P. Hyman and J. W. Medlin, J. Phys. Chem. B **109**, 6304 (2005).
[38]Y. Xie, Ch. Y. Liao, and J. Zhou, Biophys. Chem. **179**, 26 (2013).
[39]L. L. Zhu and X. J. Zheng, Eur. J. Mech. A **29**, 337 (2010).
[40]J. L. Giocondi and G. S. Rohrer, Chem. Mater. **13**, 241 (2001).
[41]J. J. Wang, F. Y. Meng, X. Q. Ma, M. X. Xu, and L. Q. Chen, J. Appl. Phys. **108**, 034107 (2010).
[42]M. Fechner, S. Ostanin, and I. Mertig, Phys. Rev. B **77**, 094112 (2008).
[43]D. Y. He, L. J. Qiao, A. A. Volinsky, Y. Bai, and L. Q. Guo, Phys. Rev. B **84**, 024101 (2011).
[44]Y. Kim, A. Kumar, A. Tselev, I. I. Kravchenko, H. Han, I. Vrejoiu, W. Lee, D. Hesse, M. Alexe, S. V. Kalinin, and S. Jesse, ACS Nano **5**, 9104 (2011).
[45]A. Ryuji, J. Phys. Soc. Jpn. **15**, 795 (1960).